

Structures and Transitions in Light Unstable Nuclei

Y. Kanada-En'yo^a, H. Horiuchi^b and A. Doté^b

^aInstitute of Particle and Nuclear Studies,
High Energy Accelerator Research Organization,
Oho 1-1, Tsukuba-shi 305-0801, Japan

^bDepartment of Physics,
Kyoto University,
Kitashirakawa-Oiwake, Sakyo-ku,
Kyoto 606-01, Japan

We study the structures of the unstable Be isotopes with the theoretical method of antisymmetrized molecular dynamics. It is found that various structures of the excited states appear in the low-energy region of neutron-rich Be nuclei. Focusing on the 2α clustering, we analyze the intrinsic structures with the help of the experimental data of Gamow-Teller transitions.

1. INTRODUCTION

Recently, the study of unstable nuclei is one of the hot subjects. In the light unstable nuclei, the experimental informations near the drip lines increase rapidly and many interesting phenomena are found. The exotic structures such as the halo, the skin structures, and the clustering structures are suggested in some light unstable nuclei. Are the features of the clusters in unstable nuclei similar to those in the stable nuclei? The shift of the magic number and the deformations of unstable nuclei are the concerned problems.

Our aim is to research on the excited states of unstable and to study systematically the various structures of unstable nuclei. We apply a theoretical method of antisymmetrized molecular dynamics (AMD). The method of variation after projection (VAP) in the framework of AMD has been already proved to be useful to investigate the excited states of light unstable nuclei [1,2] as well as stable nuclei [3]. AMD is a powerful approach which is applicable to the excited states of general nuclei. The wave function of AMD can represent various clustering structures as well as shell-model-like structures, because there is no inert core in the framework.

In the previous study on the excited states of ^{10}Be with AMD [2,4], we found that the molecule-like structures may coexist in the low-energy region with the ordinary shell-model-like states. The data of the transitions such as $E2$ and Gamow-Teller transitions are so helpful to classify the excited levels into rotational bands. The reader is referred to the paper [2] for the detailed discussions.

2. FORMULATION

In this section we explain the formulation of AMD for the study of the nuclear structure of the excited states.

2.1. Wave function

The wave function of a system is written by AMD wave functions,

$$\Phi = c\Phi_{AMD} + c'\Phi'_{AMD} + \cdots. \quad (1)$$

An AMD wavefunction of a nucleus with mass number A is a Slater determinant of Gaussian wave packets;

$$\Phi_{AMD}(\mathbf{Z}) = \frac{1}{\sqrt{A!}} \mathcal{A}\{\varphi_1, \varphi_2, \cdots, \varphi_A\}, \quad (2)$$

$$\varphi_i = \phi_{\mathbf{X}_i} \chi_{\xi_i} \tau_i : \begin{cases} \phi_{\mathbf{X}_i}(\mathbf{r}_j) \propto \exp \left[-\nu \left(\mathbf{r}_j - \frac{\mathbf{X}_i}{\sqrt{\nu}} \right)^2 \right], \\ \chi_{\xi_i} = \begin{pmatrix} \frac{1}{2} + \xi_i \\ \frac{1}{2} - \xi_i \end{pmatrix}, \end{cases} \quad (3)$$

where the i th single-particle wave function φ_i is a product of the spatial wave function, the intrinsic spin function and the iso-spin function. The spatial part $\phi_{\mathbf{X}_i}$ is presented by complex parameters X_{1i}, X_{2i}, X_{3i} , of the centers of Gaussians, and χ_{ξ_i} is the intrinsic spin function parameterized by ξ_i . τ_i is the iso-spin function which is fixed to be up(proton) or down(neutron) in the present calculations. Thus an AMD wave function is parameterized by a set of complex parameters $\mathbf{Z} \equiv \{X_{ni}, \xi_i\}$ ($n = 1, 3$ and $i = 1, A$) which determine the centers of Gaussians of the spatial parts and the directions of the intrinsic spins for all single-particle wave functions.

If we consider a spin-parity eigen state projected from a AMD wave function, the total wave function is linear combinations of Slater determinants,

$$\Phi(\mathbf{Z}) = P_{MK'}^{J\pm} \Phi_{AMD}(\mathbf{Z}) = (1 \pm P) \int d\Omega D_{MK'}^{J*}(\Omega) R(\Omega) \Phi_{AMD}(\mathbf{Z}), \quad (4)$$

where P is a parity projection operator. The integrations for the Euler angles are numerically calculated by a summation of mesh points on Ω .

In principal the total wave function can be a superposition of independent AMD wave functions,

$$\Phi = cP_{MK'}^{J\pm} \Phi_{AMD}(\mathbf{Z}) + c'P_{MK'}^{J\pm} \Phi_{AMD}(\mathbf{Z}') + \cdots. \quad (5)$$

2.2. Energy variation

We make variational calculations to find the state which minimizes the energy of the system; $\langle \Phi | H | \Phi \rangle / \langle \Phi | \Phi \rangle$ by the method of frictional cooling [5,6], one of the imaginary time methods. The time development of the wave function $\Phi(\mathbf{Z})$ is given by the equations,

$$\frac{dX_{nk}}{dt} = (\lambda + i\mu) \frac{1}{i\hbar} \frac{\partial}{\partial X_{nk}^*} \frac{\langle \Phi(\mathbf{Z}) | H | \Phi(\mathbf{Z}) \rangle}{\langle \Phi(\mathbf{Z}) | \Phi(\mathbf{Z}) \rangle}, \quad (n = 1, 3 \quad k = 1, A) \quad (6)$$

$$\frac{d\xi_k}{dt} = (\lambda + i\mu) \frac{1}{i\hbar} \frac{\partial}{\partial \xi_k^*} \frac{\langle \Phi(\mathbf{Z}) | H | \Phi(\mathbf{Z}) \rangle}{\langle \Phi(\mathbf{Z}) | \Phi(\mathbf{Z}) \rangle}, \quad (k = 1, A) \quad (7)$$

with arbitrary real numbers λ and $\mu < 0$. It is easily proved that the energy of the system decreases with time. After sufficient time steps of cooling, we obtain the optimum parameters for the minimum-energy state.

2.3. Lowest J^\pm states

In order to obtain the wave function for the lowest J^\pm state, we perform the energy variation for the spin parity eigenstates projected from an AMD wave function. In this case the trial function is $\Phi = P_{MK'}^{J^\pm} \Phi_{AMD}(\mathbf{Z})$. For the preparation of VAP calculations, first we make variational calculations before the spin projection in order to choose an initial wave function for each parity and an appropriate K' quantum for each spin-parity state. Then we perform VAP calculation for

$$\langle P_{MK'}^{J^\pm} \Phi_{AMD}(\mathbf{Z}) | H | P_{MK'}^{J^\pm} \Phi_{AMD}(\mathbf{Z}) \rangle / \langle P_{MK'}^{J^\pm}(\mathbf{Z}) | P_{MK'}^{J^\pm}(\mathbf{Z}) \rangle \quad (8)$$

with the adopted K' quantum from the initial state. In the VAP procedure, the 3-axis of Euler angle in the total-angular momentum projection is not necessarily same as the principal z -axis. The direction of the intrinsic deformation in the body-fixed frame is automatically determined in the energy variation depending on the adopted K' quantum. However, in many cases, the approximately principal axis z obtained by a VAP calculation is found to be almost equal to the 3-axis.

2.4. Higher excited states

As mentioned above, with the VAP calculation for $\Phi(\mathbf{Z}) = P_{MK'}^{J^\pm} \Phi_{AMD}(\mathbf{Z})$, we obtain the set of parameters $\mathbf{Z} = \mathbf{Z}_1^{J^\pm}$ which presents the wave function for the first J^\pm state. To search the parameters \mathbf{Z} for the higher excited J^\pm states, we make the energy variation for the orthogonal component of a spin-parity projected AMD wave function to the lower states by superposing the wave functions. If the AMD wave functions for the higher excited states have energetically local minimums, we do not need orthogonalization in VAP calculations.

2.5. Expectation values

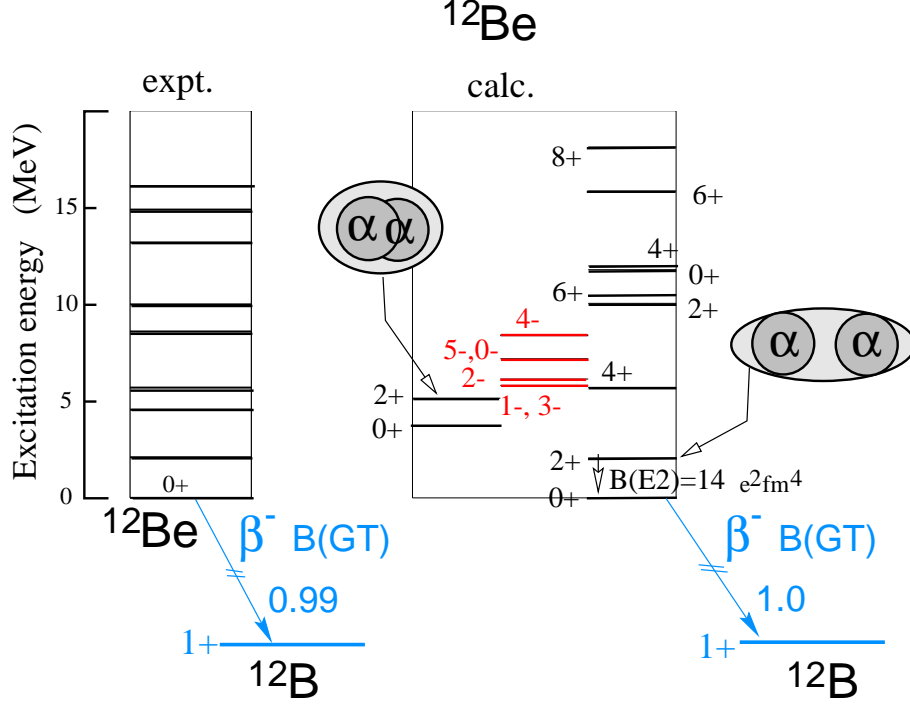
After VAP calculations for various J_n^\pm states, we obtain many intrinsic states $\Phi_{AMD}^1, \Phi_{AMD}^2, \dots, \Phi_{AMD}^m$. Finally we improve the wave functions by diagonalizing the Hamiltonian matrix $\langle P_{MK'}^{J^\pm} \Phi_{AMD}^i | H | P_{MK''}^{J^\pm} \Phi_{AMD}^j \rangle$ and the norm matrix $\langle P_{MK'}^{J^\pm} \Phi_{AMD}^i | P_{MK''}^{J^\pm} \Phi_{AMD}^j \rangle$ simultaneously with regard to (i, j) for all the intrinsic states and (K', K'') . In comparison with the experimental data, the theoretical values are calculated with the final states after the diagonalization.

3. RESULTS

We calculate the excited states of ^{12}Be and ^{11}Be . The adopted interactions are the MV1 case3 (the finite two-body and the zero-range three-body interactions [7]) for the central force, and G3RS for the spin-orbit force [8]. The coulomb interaction is approximated by a sum of seven Gaussians. In the present calculations, we adopt the Majorana parameter $m = 0.65$ and omit the Bartlett and Heisenberg terms in the two-body central force. As for the strength of the spin-orbit force, we try two cases of the parameter, $u_{ls}=3700$ MeV and $u_{ls}=2500$ MeV.

The resonance states are treated as a bound-state approximation in AMD, because the restriction of the Gaussian forms of the wave functions makes an artificial barrier for outgoing particles.

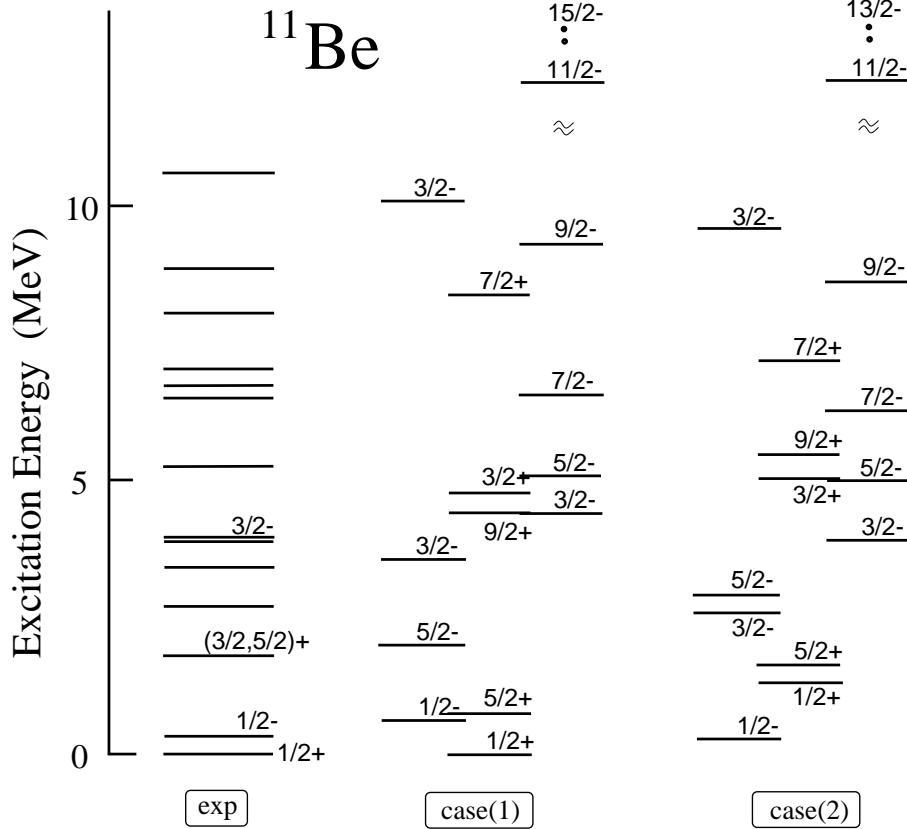
Figure 1. Energy levels and transitions of ^{12}Be . The adopted parameters for the calculations are Majorana parameter $m = 0.65$ and the strength of the spin-orbit force $u_{ls} = 3700$ MeV.



3.1. ^{12}Be

The energy levels of ^{12}Be are displayed in Figure 1. The theoretical results are calculated with the stronger spin-orbit force as $u_{ls} = 3700$ MeV which can reproduce the abnormal parity of the ground $1/2^+$ state in ^{11}Be . Many excited states are seen in the low-energy region. Even though the ^{12}Be has the neutron magic number 8, it is surprising that the calculated ground state is not the ordinary state with the neutron closed p -shell, but a 2 particle 2 hole state with the developed clustering structure. As the evidence of the breaking of the closed p -shell, the calculations reproduce well the small value of the Gamow-Teller(GT) transition strength from $^{12}\text{Be}(0^+)$ to $^{12}\text{B}(1^+)$. The experimental $B(GT)$ is about one third as small as the value expected for the closed p -shell $^{12}\text{Be}(0^+)$. In other words, the weak GT transition is one of the proofs for the disappearance of the neutron magic number 8 in neutron-rich Be isotopes. It is consistent with the shell model analysis by T. Suzuki et al. [9]. We also find many excited states with the developed molecule-like structures which construct the rotational bands $K^\pi = 0_1^+$, $K^\pi = 1_1^-$, $K^\pi = 0_3^+$ in the low-energy region. Since the ground state has the large deformation in the present calculations, The predicted $B(E2; 2_1^+ \rightarrow 0_1^+)$ in the ground band is $14 \text{ e}^2\text{fm}^4$ and is much larger than the value $7 \text{ e}^2\text{fm}^4$ of $B(E2; 2_2^+ \rightarrow 0_2^+)$ in the second $K^\pi = 0^+$ band which consists of the closed p -shell states.

Figure 2. Energy levels of ^{11}Be . The adopted parameter for the strength of the spin-orbit force is $u_{ls} = 3700$ MeV for case(1) and $u_{ls} = 2500$ MeV for case(2).



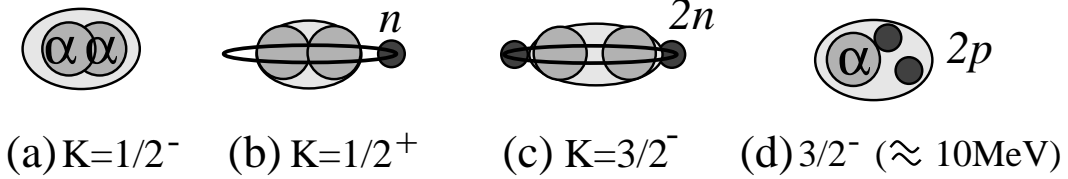
3.2. ^{11}Be

In this subsection, we discuss the excited states of ^{11}Be . In Fig 2, the calculated energy levels are shown with the experimental data. We use the rather strong spin-orbit force in case (1) and the weaker LS force in case (2). The binding energies are underestimated as 58 MeV in case (1) and as 54 MeV in case (2). It is not difficult to fit to the experimental binding energy by choosing a smaller value for the Majorana parameter.

In the case (1) with the stronger LS force, the abnormal spin-parity $1/2^+$ state comes down lower than the normal negative parity states, which is consistent with the experimental data. In both cases, we found some rotational bands $K^\pi = 1/2^-$, $K^\pi = 1/2^+$ and $K^\pi = 3/2^-$, although the order of the levels depends on the adopted interaction. The $K^\pi = 3/2^-$ band has a large moment of inertia and reaches to the high spin states. The highest spin is $15/2^-$ in case(1) and $13/2^-$ in case (2). It is expected that the $K^\pi = 3/2^-$ band may reach to the further high spin such as a $17/2^-$ state in the calculations with a smaller value of the Majorana parameter.

Next we analyze the intrinsic wave functions of the obtained rotational bands. In the results of ^{11}Be , 2α clustering structures appear very often in many states. The schematic figures are presented in Fig. 3. Two alpha cores are found in the states of the lowest

Figure 3. Schematic figures for the intrinsic structures of ^{11}Be . (a), (b), (c), (d) correspond to $K = 1/2^-$, $K = 1/2^+$, $K = 3/2^-$, $3/2^- (\approx 10 \text{ MeV})$, respectively.

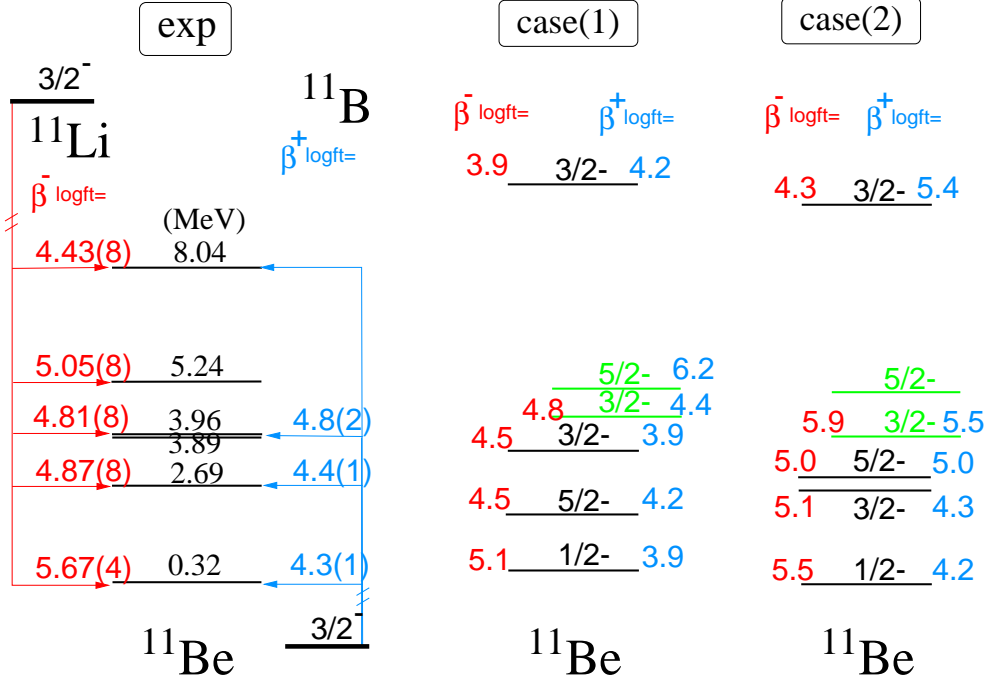


negative parity band $K^\pi = 1/2^-$ (Fig.3(a)). In the positive parity states, one neutron is in the sd orbit and the 2α clustering develops (Fig.3(b)). We think that one of the reason of the energy gain of the positive parity states is considered to be the clustering development. The interesting point is that the $K^\pi = 3/2^-$ band comes from the well-developed molecule-like structure with 2 neutrons in the sd orbit (Fig.3(c)). The large moment of inertia results from the largely deformed intrinsic structure. At about 10 MeV, we found another characteristic state where one of the 2 α -clusters completely breaks (Fig.3(d)). In this state the intrinsic spins of 2 protons couple up to be totally a unit. As mentioned above, various structures coexist in the low energy region in ^{11}Be . It is expected that the valence neutrons play important roles in these excited states.

We discuss the Gamow-Teller(GT) transitions in order to analyze the level structures of ^{11}Be . First we consider β decay from ^{11}B . The experimental data of GT-type transitions from the ground state of ^{11}B are deduced from the 0° cross sections of the charge exchange reactions [10]. Comparing the calculated $\log ft$ values with experimental data (Fig.4), the observed three levels well correspond to the excited states in the lowest $K^\pi = 1/2^-$ band. It is natural that the GT transitions from ^{11}B to these levels are reasonably strong because both the parent and the daughter states are ordinary p -shell states.

The beta decays from ^{11}Li are shown in Fig.4. We notice that the ideal 2α -cluster structures in the daughter ^{11}Be states forbid any GT transitions from ^{11}Li because of the Pauli forbidden. In other words, the GT transitions from ^{11}Li are allowed only if the daughter states of ^{11}Be have the component with the breaking of the α clusters. The calculations well agree with the experimental $\log ft$ values. According to the calculated results, the lowest $3/2^-$ and $5/2^-$ states in the $K^\pi = 1/2^-$ band have the more than 10 % breaking of the clusters. One of the reason for the weak GT transition to the lowest $1/2^-$ state is the clustering structure of ^{11}Be . Another reason is suggested by Suzuki et.al [9] as the halo structure of the parent ^{11}Li state, which may not be described enough in the present AMD calculations. In the calculations, transitions for the higher excited states in the $K^\pi = 3/2^-$ band are suppressed because of the α clusters in the developed molecule-like structures. The strong transition to the excited state at 8 MeV well fits to the calculated $3/2^-$ state ($\approx 10 \text{ MeV}$) where one of the two α clusters completely breaks.

As for the $E1$ transitions, the $B(E1; 1/2^- \rightarrow 1/2^+)$ of the present calculations is much smaller than the experimental data. We should describe the wave function more precisely to reproduce the strength $B(E1)$.

Figure 4. Beta decays to the excited states of ^{11}Be . GT transitions are calculated.

4. SUMMARY

We studied the structure of the excited states of ^{12}Be and ^{11}Be and analyzed the level structure with the help of the data of Gamow-Teller transitions.

In ^{12}Be , it is found that the ground state has the developed clustering structure instead of the neutron p -shell closed state. The main component of the ground state is the $2p$ - $2h$ state in terms of a simple shell model. That is to say the neutron magic number 8 disappears in ^{12}Be . It is consistent with the small GT strength to ^{12}Be . Many molecule-like states make rotational bands in low energy regions.

In the case of ^{11}Be , various structures are seen in the excited states. In the results rotational bands with the the developed clustering states are suggested. We discuss the Gamow-Teller transitions comparing the AMD calculations with the experimental data. The experimental data of GT transitions from ^{11}B well agree with the theoretical results of the decay to the ordinary p -shell states of ^{11}Be . With the help of the $\log ft$ values for the transitions from ^{11}Li , we can estimate the dissociation of α clusters in the daughter ^{11}Be nucleus. The observed strong GT transitions from ^{11}Li to ^{11}Be at 8 MeV comes from the breaking of the one of the 2 α clusters in the excited state of the daughter nucleus ^{11}Be .

REFERENCES

- [1] Y. Kanada-En'yo, H. Horiuchi and A. Doté, J. Phys. G, Nucl. Part. Phys. **24** 1499 (1998).

- [2] Y. Kanada-En'yo, H. Horiuchi and A. Doté, Phys. Rev. C **60**, 064304 (1998)
- [3] Y. Kanada-En'yo, Phys. Rev. Lett. **81**, 5291 (1998).
- [4] A. Doté, H. Horiuchi, and Y. Kanada-En'yo, Phys. Rev. C **56**, 1844 (1997).
- [5] Y. Kanada-En'yo, A. Ono, and H. Horiuchi, Phys. Rev. C **52**, 628 (1995); Y. Kanada-En'yo and H. Horiuchi, Phys. Rev. C **52**, 647 (1995).
- [6] Y. Kanada-En'yo and H. Horiuchi, Prog. Theor. Phys. **93**, 115 (1995).
- [7] T. Ando, K. Ikeda, and A. Tohsaki, Prog. Theor. Phys. **64**, 1608 (1980).
- [8] N. Yamaguchi, T. Kasahara, S. Nagata, and Y. Akaishi, Prog. Theor. Phys. **62**, 1018 (1979); R. Tamagaki, Prog. Theor. Phys. **39**, 91 (1968).
- [9] T. Suzuki and T. Otsuka, Phys. Rev. C **50**, R555(1994); T. Suzuki and T. Otsuka, Phys. Rev. C **56**, 847 (1997).
- [10] I. Daito, et al., Phys. Lett. B **418** 27 (1998).
- [11] N. Aoi, et al., Nucl. Phys. A **616** 181c (1997).